ORIGINAL PAPER

Permeability control and flood risk assessment of urban underlying surface: a case study of Runcheng south area, Kunming

Tong Xu[1] · Zhiqiang Xie[1] · Fei Zhao[1] · Yimin Li[1] · Shouquan Yang[2] · Yangbin Zhang[2] · Siqiao Yin[2] · Shi Chen[3] · Xuan Li[4] · Sidong Zhao[4] · Zhiqun Hou[5]

Abstract

Because of climate change and rapid urbanization, urban impervious underlying surfaces have expanded, causing Chinese cities to become strongly affected by flood disasters. Therefore, research on urban flood risks has greatly increased over the past decade, with studies focusing on reducing the risk of flood disaster. From 2012 to 2020, the impervious underlying surface has increased, and the permeable underlying surface has decreased annually in Kunming City. This study was conducted to investigate the impact of continuous changes in the urban underlying surface on flood disasters in the Runcheng area south of Kunming City from 2012 to 2020. We constructed a two-dimensional flood model to conduct flood simulations and flood risk analysis for this area. The relationship between the permeability of the underlying surface and urban flood risk was simulated and analyzed by varying the urban underlying surface permeability (0–60%). The simulation results show that the model can accurately simulate urban waterlogging, and the increase in urban waterlogging risk is related to the underlying surface permeability. Urban flood risk decreases with the increase in permeable underlying surface. The increase rate of flood risk in the part with permeability of 0–35% is greater than that the part with permeability of 35–60%, that is, when the permeability of underlying surface is lower than 35%, the flood risk rate will be higher. We demonstrated the impact of the urban underlying surface permeability on the risk of urban flood disasters, which is useful for urban planning decisions and urban flooding risk controls.

Keywords Urbanization · Urban flood disaster · Flood risk analysis · Permeable underlying surface · Hydro-hydrodynamic model

✉ Zhiqiang Xie
  xzq_2019@ynu.edu.cn

1 School of Earth Sciences, Yunnan University, Kunming 650504, China

2 Institute of International Rivers and Eco-Security, Yunnan University, Kunming 650504, China

3 Kunming Dianchi Investment Co., Ltd, Kunming 650504, China

4 Kunming Drainage Facilities Management Co., Ltd, Kunming 650504, China

5 Kunming Urban Underground Space Planning and Management Office, Kunming 650504, China

1 Introduction

In recent years, global warming has increased, extreme weather has occurred more frequently, and urban flooding has become more likely to occur. With continuous urbanization, the water surfaces of cities have decreased, and their impervious surfaces have increased. Increases in the impermeable surfaces reduce the absorption capacity of urban surfaces for rainwater, shorten the duration of surface runoff formation, and intensify the "Rain Island Effect." The permeability of underlying surfaces of cities has decreased continuously, such that the urban areas of some cities have permeabilities below 30%. When a rainstorm occurs, the drainage and infiltration capacities of a city with a low underlying surface permeability are insufficient to cope with the scale of rainfall, increasing the risk of urban flood disasters. From 1989 to 2018, 3945 major flood disasters occurred worldwide. China, India, the USA, and Indonesia experienced the most frequent disasters, with a total of ~1200 events. According to Emergency Events Database statistics, 109 flood disasters occurred in 2018, with a relatively small number of flood deaths (1995) and victims (12.62 million).

Urban flood disasters result in serious population and economic losses. From 2008 to 2010, approximately 137 cities experienced more than three floods, and nearly 58 cities experienced more than 12 h of disastrous flooding during a single precipitation event from 2008 to 2010 (Liang 2016). On July 21, 2012, a torrential rainstorm occurred in Beijing, resulting in 79 deaths, the collapse of 10,660 houses, and damage to 163 immovable cultural relics, with 1.602 million victims, traffic losses of 11.64 billion yuan, congestion, and road interruptions. In the past five years, more than 300 cities in China have experienced various degrees of flood disasters characterized by wide ranges, long-term ponding, serious subsequent impacts on urban development and management, and huge losses of life and property. In August 2018, more specifically, August 18–19, Typhoon "Winbia" caused torrential rain in Shouguang City, Shandong Province, China. Many villages along the Mihe River in Shouguang City were flooded, and many buildings, farmland, greenhouses, and breeding farms were affected by the flood, which resulted in heavy losses and caused serious impacts on urban roads and populations that resulted in economic losses as high as 9.2 billion yuan. Because of rapid urbanization and the effects of climate change, the frequency of flooding has increased, and the impact of flooding has become increasingly extensive (Shi 2012; Quan 2014). Rapid urbanization increases in the impervious underlying surface, population growth is the main reason for urban flooding in China (Yin et al. 2015), and flood disasters have become a common concern for the Chinese government and the public.

At present, the research on urban flood models can be divided into three categories: hydrological model, hydrodynamic model, and simplified model (Xia et al. 2018; Qi et al. 2021). Different models have their own advantages and disadvantages. The Storm Water Management Model (SWMM), a dynamic rainfall and runoff simulation model, is a representative hydrological model, but it has high data requirements and limitations; the hydrodynamic model uses differential equations to calculate the flow movement, so the accuracy is high, but the operation speed is low (Rong et al. 2020). Other simplified models, such as cellular automata (CA), have become popular in the field of hydrological model research due to their low data requirements and high operation speed (Li et al. 2020; Wang et al. 2020a, b). Many scholars have conducted in-depth research and exploration on urban flood and waterlogging and have made good progress in its simulation and treatment. The concept of low impact development (LID) and the concept of "sponge city" have been

proposed to divert and control urban runoff in order to alleviate urban floods (Sun et al. 2020; Chen et al. 2020). Most scholars mainly simulate urban flood disasters through rainstorm and flood management model (SWMM), Mike, InfoWorks ICM and other software (Xu et al. 2019; Seenu et al. 2019; Bisht et al. 2016), to study the inundation algorithm of urban rainstorm and ponding on the ground (Hou and Du 2020; Huang and Jin 2019; Meng et al. 2019; Liu et al. 2020). Some scholars have also constructed an urban comprehensive watershed drainage model based on InfoWorks ICM; selected different measured rainstorms for simulation analysis studied the effects of drainage capacity, ground ponding depth, and duration on the drainage pipe network system under different rainstorm return periods (Huang et al. 2017; Wang 2018; Wang et al. 2020a, b) and analyzed it based on multi-model coupling (Li et al. 2019; Cheng et al. 2017; Geng et al. 2019) and flood risk assessment (Hu et al. 2017; Zhu et al. 2019; Chakraborty and Mukhopadhyay 2019).

For research on the permeability of underlying surfaces in urban areas, some scholars use the measured underlying surface permeability parameters to fit the model (Hossain Anni et al. 2020), or use the impervious underlying surface to explore the urbanization process (Peng et al. 2016; Yu et al. 2018). Some scholars have used six different years (1966, 1971, 1976, 1981, 1986, and 2000) and six simulated land-use scenarios (0%, 20%, 40%, 60%, 80% and 100% of impermeable surface area percentage) to input into the coupled hydrological and hydraulic model to study the impact of urbanization on urban flood risk change (Feng et al. 2021).

In summary, it is a good decision to choose the hydrological hydrodynamic model to simulate urban flood because the hydrological hydrodynamic model can not only simulate the state of one-dimensional underground pipe network, but it can also simulate the water situation of two-dimensional ground areas. The InfoWorks ICM software has a good calculation accuracy for flood numerical simulation; thus, the InfoWorks ICM software was selected as the simulation software in this study. InfoWorks ICM is a software developed by the HR Wallingford company in the UK; it can realize the coupling of the urban drainage pipe network system model and the river channel model. It can more realistically simulate the interaction between underground drainage pipe network system and surface storage water bodies. The fully solved Saint–Venant equation was used to simulate pipeline open channel flow, and the Preissmann slot method was used to simulate the open channel overload, as it can simulate various complex hydraulic conditions, use the storage capacity to reasonably compensate and reflect the pipe network reserves, and avoid the wrong prediction of pipeline overload and flood disaster.

Urban flood disaster is one of the major problems in urban areas, and they pose a great threat to society and personal safety every year. Therefore, managing urban floods is crucial, and this problem needs to be solved urgently through urban development. Their management and transformation have also become the focus of current urban problem research (Kong et al. 2021). The frequent occurrence of urban flood events has exposed some problems in the process of urbanization, such as the rapid development of the city, annual increases in the area of houses and roads, aging and deterioration of drainage pipeline systems and other infrastructure, and obvious problems in the normal operation capacity and maintenance capacity of urban underground drainage pipelines. This study focuses on the impact of urbanization on urban flood disaster from the perspective of underlying surface permeability, simulates scenarios with varying permeabilities of underlying urban surfaces through the InfoWorks ICM drainage flood model, and evaluates the impact of changes in urban underlying surfaces on the urban flood disaster risk under different rainfall scenarios, so as to provide informed opinions on urban underlying surface permeability for urban flood risk control.

2 Study area and data

2.1 Study area

Runcheng south area is located in the south of Panlong District, Kunming City, Southwest China and on the Yunnan–Guizhou Plateau. The terrain of the study area is high in the north and low in the south, gradually decreasing in a ladder shape from the north to south. It has an altitude of about 1891 m, and the study area covers an area of 7.64 km² (Fig. 1). Runcheng is the transportation hub of the old and new cities of Kunming. It is surrounded by Rixin Road, Qianxing Road, and Qianwei West Road, connecting Guangfu Road, Guannan Avenue, the second ring road and other main roads. By 2019, Kunming had a total area of 21,473 square kilometers, a built-up area of 483.52 square kilometers, a permanent resident population of 6.95 million, an urban population of 5.1152 million, and an urbanization rate of 73.6%. The month with the most rainfall in Kunming is about July and August every year. In July 2019, the rainfall in Kunming was 279.87 mm, while in July 2018, the rainfall in Kunming was only 159.51 mm, 120.36 mm more than that in the same period in history. Every rainy season, Kunming suffers from serious urban floods, resulting in significant social and economic losses and environmental disasters. Besides, this is seriously damaging to the city's reputation. Over the last ten years, the economy of Runcheng area has developed rapidly, and the impervious underlying surface has increased annually. In recent years, serious flood disasters have occurred often in this area. Therefore, this area is a typical urban flood research area.
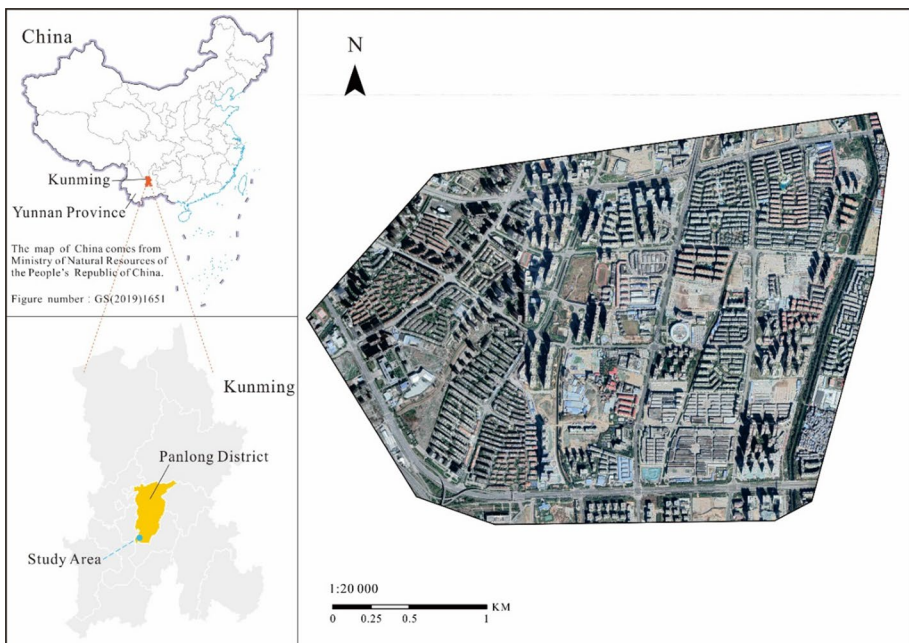
Fig. 1 Geographical location of Runcheng in the south of Kunming

2.2 Data

2.2.1 GIS data

The experimental data were mainly provided by the underground pipeline detection and Management Office of Kunming City and included underground drainage pipeline data, rainfall measurements, RS imagery, digital elevation model data, historical waterlogging location information, and other data, as shown in Table 1. The original geophysical data included inspection well coordinates, elevations, pipe diameters, pipe bottom elevations, and pipe top elevations, which were the most recent data (collected in 2018).

2.2.2 Image data

Remote sensing image data include satellite image data of Kunming in 2012 and 2020. These images have a resolution of 0.5×0.5 m and were derived from Google Earth. Remote sensing image data can be used for underlying surface analysis. ENVI software was used for analysis and extraction. The analysis method was the maximum likelihood method in supervised classification. After this, ArcGIS software was used to manually correct the classification results and manually correct the wrong points and missing points. The underlying surface was analytically generalized into the following six categories: road, building, green space, bare soil, hardened surface, and water body. Field verification and comparison of random sampling demonstrate that the classification results are consistent with the real values. Buildings and hardened ground surfaces hinder the infiltration of rainwater, and the water permeability of green spaces is generally higher than that of bare soil. Therefore, in order to make the model simulation results more accurate, it is necessary to modify the infiltration rates and other parameters according to the different underlying surfaces.

The underlying surfaces in the study area are shown in Fig. 2a, b, which are the results of RS image analyses of data from 2012 and 2020, respectively. Figure 2 shows that, with the gradual development and utilization of urban land resources, the yellow bare soil sections later became buildings and roads. According to the underlying surface results, the proportion of permeable underlying surfaces gradually decreased from 47 to 31%, from 2012 to 2020, while the proportion of impervious underlying surfaces increased from 53 to 69% (a 16% increase in area), which is an important factor in flood disasters in most cities.

Table 1 Data list

| Data type	Data content
Geophysical data of rainwater and sewage drainage pipeline	Inspection well coordinate, elevation, pipe position, pipe diameter, pipe bottom elevation
Rainfall data	Measured rainfall data collected from a rain gauge near Runcheng area in the south of Kunming
Historical waterlogging prone point information	Including the depth, time, and scope of ponding
Remote sensing image data	Image data of Kunming City in 2012 and 2020, from Google Map, 0.5×0.5 m resolution ratio
Digital elevation model data	Ground elevation point data
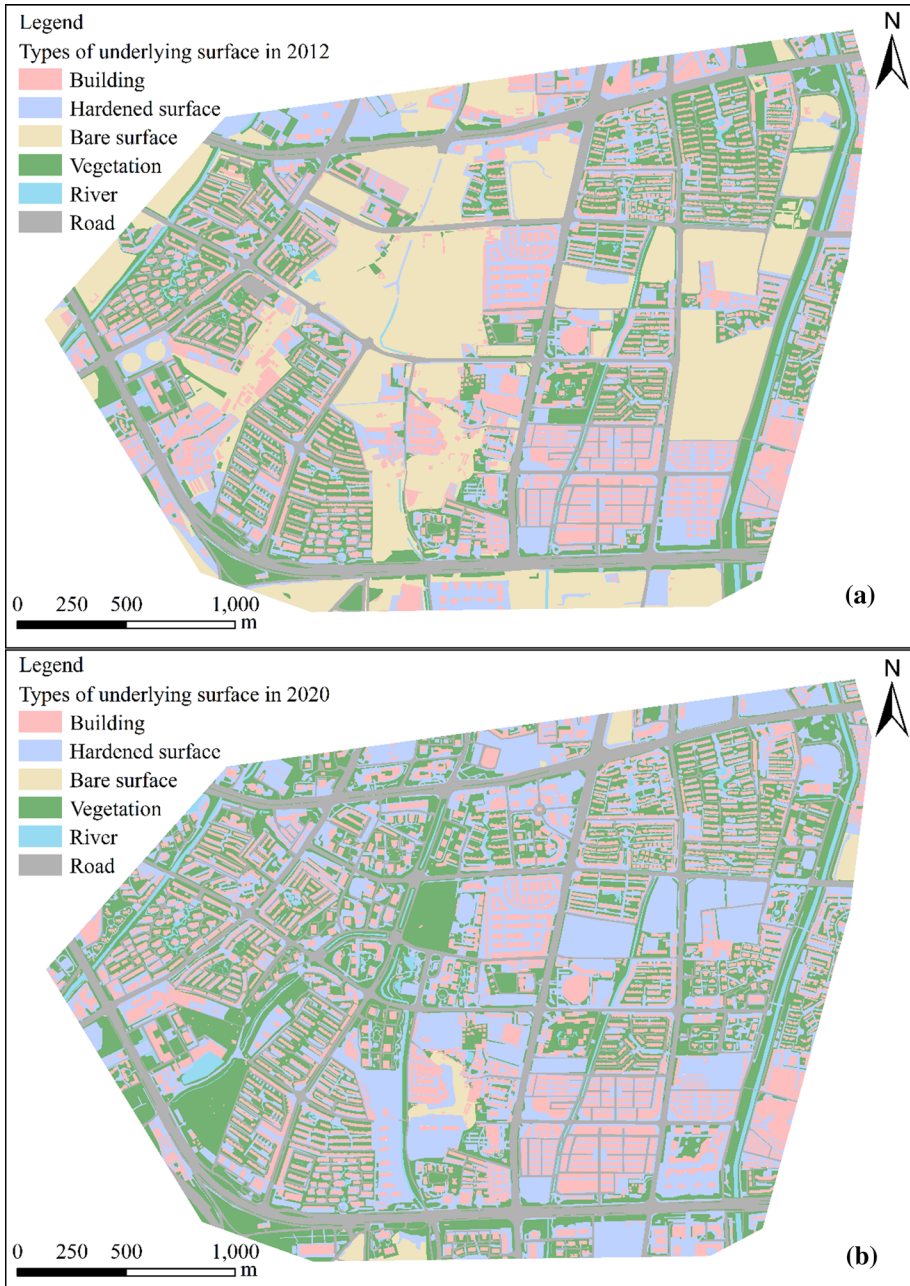
Fig. 2 Underlying surfaces of the study area in 2012 and 2020

2.2.3 Rainfall data

Rainfall data mainly include measured rainfall data and rainfall model generated by rainstorm intensity formula. Different types of rainfall have different influences on the underlying surface, making it necessary to select representative rainfall events. The rainfall data used in this study were collected at Wuda village station in Kunming on August 16, 2020 (Wuda village station is in the northern part of the study area), at an interval of 5 min, yielding a total rainfall of 99 mm. In addition, short-term rainfall data were generated by using the rainstorm intensity formula in Kunming City, with recurrence periods of 1, 2, 3, 5, and 10 years, respectively. These values were used as the boundary conditions for simulation.

The rainstorm model selected for this study was the Chicago rainstorm model (Keifer and Henry 1957). A heterogeneous synthetic rainstorm process line model was proposed according to the relationships between rainfall intensity, duration, and frequency (Chicago rainfall process line model), which has been widely used. The rainstorm intensity formula is as follows:

$$q = \frac{167A_1(1 + C\lg P)}{(t + b)^n} \tag{1}$$

where Q is rainstorm intensity (L/(s hm^2)), A_1 is the rainfall in different return periods (mm), C is the rainfall variation parameter, P is the rainfall return period (a), T is the rainfall duration (min), and B and n are constants reflecting changes in the designed rainfall intensity over time. For a specific return period, the molecular $A_1(1 + C\lg P)$ of the rainstorm intensity formula is a constant, set as a.

The Kunming rainstorm intensity formula (2015 version) was derived from the notification of Kunming Dianchi Administration on the issue of the Kunming rainstorm intensity formula (2015 version) issued by the Kunming Flood Control and Drought-Relief Headquarters Office of the Kunming Meteorological Bureau (No. 3 of Kunming Qi Lianfa [2015]). The rainstorm intensity formula for Kunming City is:

$$q = \frac{1226.623 \times (1 + 0.958\lg P)}{(t + 6.714)^{0.648}} \tag{2}$$

The data used to generate this formula were the minute-scale rainfall data from the Kunming National Benchmark Climate Observation Station (1981–2014) and are mainly applicable to the downtown area of Kunming.

3 Methods

3.1 Model principle

In this study, simulation was performed using the hydro-hydrodynamic model, which is a dynamic wave model used to solve the one-dimensional (1-D) Saint–Venant equations. The 2-D inundation model was based on triangulated irregular network to solve the shallow water equation using the finite volume method. The InfoWorks ICM integrated watershed drainage system model, which is capable of 1-D and 2-D simulations,

has been used widely for drainage system status assessments, urban flood disaster prediction assessments, controlling urban rainfall and runoff, and storage design evaluations. Using the 1-D urban drainage pipe network hydraulic model for the drainage system, 1-D river system hydraulic model, 2-D city/flooded river basin flood model for the city water cycle, complete system simulation to achieve the urban drainage pipe network system model, and river model integration, a more realistic simulation of the underground drainage pipe network and interactions between the receiving water body and network can be constructed. The main modules of the model included: a drainage pipe network hydraulic model (a hydrological module, pipeline hydraulic module, and sewage volume calculation module), river channel hydraulic model, 2-D urban flood and inundation model, real-time control module, water quality module, and sustainable structures module.

The hydrological calculation module adopts a distributed model to simulate rainfall runoff and carries out runoff calculations based on detailed spatial divisions of subsets of water areas and surface compositions with different runoff characteristics. In this study, this module was used to build and simulate the production and confluence of a subset of the water area. For the runoff generation model, the Horton model was selected, which involves fewer parameters and is suitable for small watersheds. For the confluence model, the SWMM nonlinear equation was selected, which has clear physical concepts and high calculation accuracy:

$$\frac{\partial A}{\partial t} + \frac{\partial Q}{\partial x} = 0, \tag{3}$$

$$\frac{1}{g}\frac{\partial v}{\partial t} + \frac{v}{g}\frac{\partial v}{\partial x} + \frac{\partial z}{\partial x} = -\frac{\tau}{\gamma R}, \tag{4}$$

$$\frac{\partial h}{\partial t} + \frac{\partial (hu)}{\partial x} + \frac{\partial (hv)}{\partial x} = q_{1D}, \tag{5}$$

$$\frac{\partial hv}{\partial t} + \frac{\partial}{\partial x}\left(hv^2 + \frac{gh^2}{2}\right) + \frac{\partial (huv)}{\partial y} = S_{0,x} - S_{f,x} + q_{1D}v_{1D}, \tag{6}$$

$$\frac{\partial hv}{\partial t} + \frac{\partial}{\partial y}\left(hv^2 + \frac{gh^2}{2}\right) + \frac{\partial (huv)}{\partial x} = S_{0,y} - S_{f,y} + q_{1D}v_{1D}, \tag{7}$$

where A is the area of the water crossing section, Q is the discharge, t is the time, x is the length in the runoff direction, and v is the velocity in the x direction. Z is the water level, g is the gravitational acceleration, τ is the average shear stress around the wet section, γ is the density of water, and R is the hydraulic radius of the wet section. H is the water depth, u is the velocity in the y direction, q_{1D} is the areal discharge, $S_{0,x}$ and $S_{0,y}$ are the slopes in the x and y directions, respectively, $S_{f,x}$ and $S_{f,y}$ are the resistance slopes in the x and y directions, respectively, and U_{1d} and V_{1d} are the velocity components of Q_{1d} in the x and y directions, respectively.

There are many runoff models, among which the Wallingford fixed runoff model is based on the calculation of runoff volumes in the UK. According to the parameters of development density, soil distribution type, and pre-stage humidity of the sub-catchment area, the runoff coefficient is predicted by a regression equation. We adopted Horton's

empirical model of surface permeability, which can generally be expressed as a time-related function. Horton's formula is as follows (Abulkadir et al. 2011):

$$f = f_0 + (f_c - f_0) * e^{-kt} \tag{8}$$

where f is the infiltration rate (mm/h), f_c is the initial infiltration rate (mm/h), f_0 is the stable infiltration rate or limit infiltration rate, K is the exponential parameter (1/h), and T is the infiltration time (h).

The hydrological calculation module and 1-D drainage system hydraulic calculation module were used to build the rainwater system model. The 2-D urban/watershed ground flood evolution module was used to simulate and evaluate the surface water. To select experimental parameters, we also measured the infiltration rate of grassland and bare land in the study area by performing a double-ring instrument experiment and calculated the attenuation coefficient. The experimental principle of double-loop instrument is to inject water into the surface loose rock within a certain hydrogeological boundary to make the infiltration water reach a stable level, that is, when the infiltration water per unit time is approximately equal, the permeability coefficient (S) value can be calculated by using the principle of Darcy's law (Hou 2019). Darcy's Law is as follows:

$$S = Q/AI \tag{9}$$

where Q is steady seepage flow (m³/min), S is the permeability coefficient (M/min), A is the inner diameter area of the double loop (m²), and I is the hydraulic gradient.

In this paper, the total risk of waterlogging was used to compare the risk changes under different permeability conditions. The total value of waterlogging risk is the product of the area of low-risk, medium-risk, and high-risk levels and the corresponding weight. Referring to the flood depth–loss curve of Shanghai construction area, combined with the current construction status and topographic elevation distribution of Runcheng south area, the weight is expressed by the loss coefficient of construction area. The calculation formula of waterlogging total risk (R) is as follows:

$$R = L \times w_1 + M \times w_2 + H \times w_3 \tag{10}$$

R represents waterlogging total risk, L represents low-risk area (m²), M represents medium-risk area (m²), H represents high-risk area (m²); $W1$, $W2$, and $W3$ are the weights corresponding to low-risk, medium-risk, and high-risk areas respectively, which are scored by experts according to experience.

3.2 Modeling process

The InfoWorks ICM software realizes the coupling of one-dimensional and two-dimensional models. The ponding area is determined through the one-dimensional model, and then, the one-dimensional and two-dimensional models are coupled to study and calculate the ponding volume, flow direction, and depth in the ponding area. It is cost-effective in terms of modeling time and model accuracy. In this study, the application of this module was used to simulate the surface ponding and analyze the flood risk. The flood model was constructed by comprehensively using the data of terrain, river channel, and pipe network. Based on the pretreatment of drainage pipe network data and analysis of the underlying surface, the pipe network model and hydrological model were constructed, respectively, and the sub-models were coupled to form a comprehensive urban flood model. On this

basis, the rationality of the model was verified by using the measured rainfall, and the multi-scenario simulation analysis was carried out in combination with the design rainstorm under different working conditions to complete the risk assessment of flood in the pipe network area.

Hydrological models usually include the runoff generation model and confluence model. The runoff generation model represents the runoff of rainwater on the ground, and the confluence model represents the velocity of rainwater runoff. To establish a hydrological model, first, the sub-catchment area needs to be divided. This can be done by roughly dividing it with Tyson polygons and then manually adjusting it in combination with the terrain, roads, distribution of rainwater pipelines in the community and GIS spatial analysis method.

According to the distribution of underlying surfaces in Kunming, the runoff generation and concentration coefficients of six types of runoff surfaces were set (Table 2). Compared with using the same fixed runoff coefficient for the whole area, this method can more accurately reflect the runoff characteristics of different catchment areas and ensure that the simulation results are more accurate and reliable. The runoff generation process of impervious surfaces is relatively stable, and thus, the runoff coefficient method was used to predict rainwater runoff. According to the technical guide for sponge city construction and codes for outdoor drainage (2016 Edition) (GB 50014-2006), the road runoff coefficient is 0.9, roof runoff coefficient is 0.9, and unused land runoff coefficient is 0.45. The runoff generation process for permeable surfaces is relatively complex. In the rainfall process, the soil infiltration capacity decreases over time and runoff generation coefficient increases. Therefore, the fixed runoff coefficient method cannot reasonably simulate the runoff generation process for permeable surfaces. The Horton runoff generation model was therefore used to simulate the runoff generation process for permeable surfaces.

Model coupling means that the sub-models were coupled to achieve water exchange among the sub-models. The 1-D hydraulic model was used to simulate the flow movement in the channels of the pipe network, whereas the 2-D surface model was used to simulate the overflow evolution of surface water and interaction process between the inspection wells and surface flooding. This included coupling the surface production and confluence model with the pipe network confluence model, coupling the pipe network confluence model with the 2-D surface overflow model, coupling the pipe network confluence model with the channel confluence model, and coupling the channel confluence model with the 2-D surface overflow model.

3.3 Model calibration and validation

3.3.1 Model calibration

The model was calibrated by inputting the measured data into the model for simulation and then comparing the results to the actual measurements. After the drainage model was established, it was necessary to check and revise the model by comparing the simulated data with the measured data. According to the collected rainfall data and ponding data, the accuracy of the model was verified by using the measured rainfall data from Wuda village station in the Runcheng area of Kunming City on August 16, 2020. The beginning time of rainfall was 22:00 h on August 16, and the ending time was 0:00 h on August 18. The measured rainfall curve is shown in Fig. 3. The rainfall gradually increased from around 2:00 h on August 17, reaching a peak at around 4:00 h, after which it gradually decreased.

Table 2 Runoff and concentration coefficients

| Underlying surface type	Runoff generation model	Fixed runoff coefficient	Initial infiltration rate	Steady seepage rate	Decay rate	Confluence model	Manning coefficient
Road	Fixed	0.9	–	–	–	SWMM	0.015
Building	Fixed	0.9	–	–	–	SWMM	0.015
Vegetation	Horton	–	227	110	2.0	SWMM	0.200
Bare surface	Horton	–	77	46	2.5	SWMM	0.200
Hardened surface	Fixed	0.8	–	–	–	SWMM	0.040
River	Fixed	1.0	–	–	–	SWMM	0.002
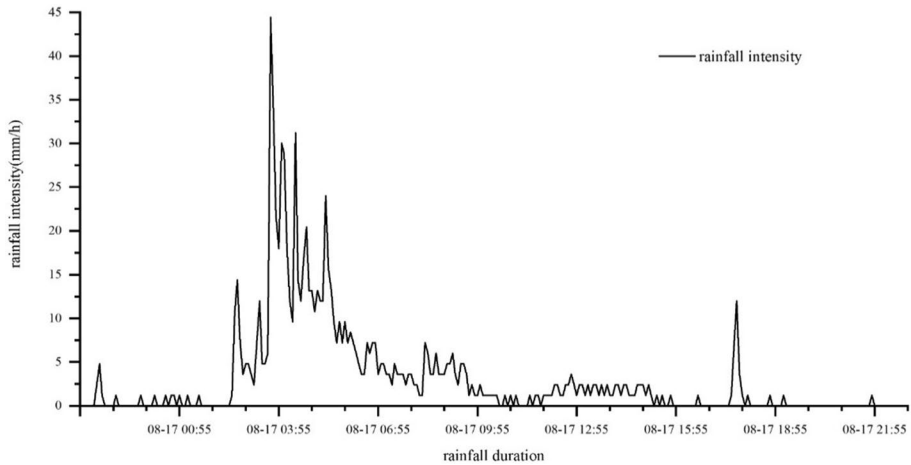
Fig. 3 Rainfall curve measured at the Wuda Village 816 site in the southern part of Kunming
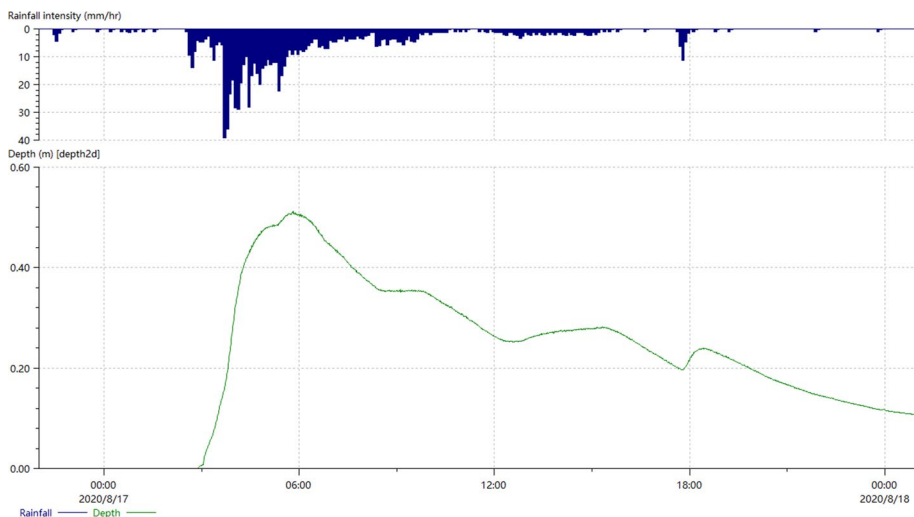
Fig. 4 Diagram of simulated flooding depths at the Wuda Village 816 site in the southern part of Kunming

As shown in Fig. 4, the maximum submerged depth was ~0.52 m, whereas the average submerged depth was ~0.4 m. At 4 h after the rainfall began, the underground drainage pipe gradually filled, and the road surfaces began to accumulate water. The water level peaked at 6 h, after which the rainfall gradually decreased and water level gradually decreased. However, the time during which water accumulated occurred later than the peak rainfall time, with a certain hysteresis.

The collected water data were limited and could only be obtained from the Internet, media, and citizens taking photographs to determine the water situation and depth. By investigating network information and Kunming City news reports, we found that the main flooding point was at the intersection of Guangfu Road and Qianwei West Road and that
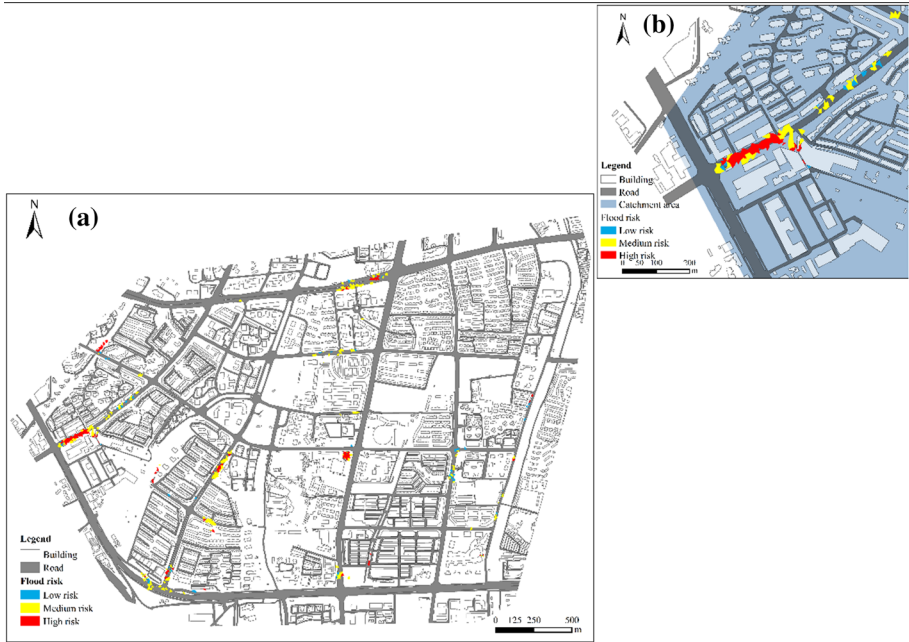
Fig. 5 Simulated diagram of accumulated water at the intersection of Guangfu and Qianwei West Roads

the water depth was ~40 cm. By importing the measured rainfall data from Wuda Village on August 16, 2020, into the model, the intersection of Guangfu and Qianwei West Roads was selected as the monitoring point in the operation results. A curve of the flooded depth in this location over time (Fig. 4) and the flooding scenario in a 2-D plane (Fig. 5a) were obtained. According to comparative analyses, the results of the model were consistent with the statistical flooding data. The water scenario at the intersection of Guangfu and Qianwei West Roads (Fig. 5b) was consistent with that of the collected water data, and the average water depth was ~0.4 m, verifying the accuracy of the model.

3.3.2 Parameter calibration

The infiltration rate is defined as the amount of water that infiltrates the soil per unit area and unit time, also known as the infiltration intensity (mm/min or mm/h). The infiltration rate under sufficient water supply conditions is known as the infiltration capacity. Soil infiltration laws are typically described quantitatively by the changes in the infiltration rate or capacity over time. The infiltration rate of dry soil decreases over time under sufficient water supply conditions, known as the infiltration capacity curve or infiltration curve. In the initial infiltration stage, infiltrating water is absorbed by soil particles and fills soil pores. This initial infiltration rate is very high. Over time and with increased seepage, the soil moisture content increases gradually, and the infiltration rate decreases. When the soil pores are full of water and infiltration is generally stable, the infiltration rate is referred to as the steady infiltration capacity or steady infiltration rate. The attenuation process from the initial permeability velocity to the stable permeability is determined by the attenuation coefficient K in Horton's formula (Eq. 8).

Table 3 Measured and simulated underground seepage rates

Time (h)	Measured infiltration rate (mm/h)	f_o (initial infiltration rate (mm/h)	f_c (steady infiltration rate (mm/h)	f_1 ($k=1$)	f_2 ($k=1.5$)	f_3 ($k=2$)	f_4 ($k=2.5$)	f_5 ($k=3$)
0:05:22	227.75	227	110	216.98	212.31	207.83	203.55	199.46
0:11:50	189.01	227	110	206.05	197.03	188.86	181.45	174.74
0:18:56	172.15	227	110	195.33	182.88	172.24	163.15	155.39
0:27:47	138.11	227	110	183.63	168.41	156.34	146.76	139.16
0:35:33	157.37	227	110	174.69	158.10	145.77	136.60	129.78
0:43:15	158.74	227	110	166.90	149.68	137.67	129.29	123.45
0:52:27	132.85	227	110	158.81	141.52	130.36	123.15	118.49
1:01:37	133.34	227	110	151.89	135.07	125.00	118.97	115.37
1:08:55	133.95	227	110	147.09	130.88	121.76	116.62	113.72
1:18:35	126.44	227	110	141.57	126.40	118.52	114.42	112.30
1:24:08	110.11	227	110	138.78	124.27	117.08	113.51	111.74

Table 4 Measured and simulated bare groundwater permeability values

Time (h)	Measured infiltration rate (mm/h)	f_o (initial infiltration rate (mm/h)	f_c (steady infiltration rate (mm/h)	f_1 ($k1 = 1$)	f_2 ($k = 1.5$)	f_3 ($k = 2$)	f_4 ($k = 2.5$)	f_5 ($k = 3$)
0:07:00	77.36	77	46	73.17	71.44	69.82	68.30	66.88
0:19:39	52.01	77	46	68.34	64.96	62.102	59.67	57.60
0:30:13	57.83	77	46	64.73	60.56	57.32	54.80	52.84
0:41:55	52.23	77	46	61.41	56.87	53.66	51.40	49.81
0:54:52	47.19	77	46	58.42	53.86	50.97	49.15	47.99
1:08:04	46.29	77	46	56.10	51.77	49.29	47.88	47.07
1:21:10	46.65	77	46	54.12	50.16	48.13	47.09	46.55

To ensure that the model infiltration rate and other parameters are suitable for local use, six different points were selected in the study area, and soil infiltration rate experiments were carried out by using a double-loop experiment. Tables 3 and 4 show the records of the measured infiltration rate of two points in the study area and records based on the simulated value of the Horton attenuation coefficient K, respectively. According to the measured values and Houghton simulation results, the Nash–Sutcliffe efficiency coefficient (NSE) was used to calculate the soil infiltration rate and verify the rationality of the model. In general, NSE values > 0.7 indicate a high degree of fit for the model. An NSE coefficient close to 1 indicates a better simulation effect. Nash's formula is as follows:

$$\text{NSE} = 1 - \frac{\sum_1^n (Q_0^t - Q_i^t)^2}{\sum_1^n (Q_0^t - Q^-)^2} \tag{11}$$

where Q_0^t and Q_i^t are the measured and simulated values at time step i, and n is the total number of time steps.

Table 5 shows the calculated values of the attenuation coefficients of green land and bare land and their NSE values. When $k = 2$, the NSE value of green space reached a maximum value of 0.85. When $k = 2.5$, the maximum NSE value for bare land was 0.77. At this time, the simulated results of the model were most similar to the measured data.

The model was constructed based on real pipe network data, localized parameters, and measured rainfall data, and the actual scenario was restored as much as possible. For pipe network data, only the main municipal road was retained, whereas redundant and insignificant rainwater grates and other small branches on both sides of the road were removed. Localized checking parameters were also adopted in setting the model parameters, and the rainfall data were derived from the measured data. To ensure the authenticity of the model, the running speed of the model was greatly increased.

4 Results

4.1 Flood risk analysis

According to the Code for Outdoor Drainage Design (GB20014-2006), 2014 edition, the depth of road water in the "Design Standard for Surface Water" refers to the depth of water at the lowest elevation of the road surface. When the depth of the water on the road exceeds 15 cm, the lane may be completely interrupted by the shutdown of motor vehicles. Considering the safety of pedestrians after increases in water levels, a water depth of 0.5 m was used as another water-level classification. The degree of water accumulation in the central urban area of Kunming City was divided into three grades: low, medium, and high risks (Table 6).

Table 5 Attenuation coefficients (k) of green land and bare land and their corresponding NSE values

NSE	e1 ($k=1$)	e2 ($k=1.5$)	e3 ($k=2$)	e4 ($k=2.5$)	e5 ($k=3$)
Green land	0.49	0.84	0.85	0.74	0.60
Bare land	0.06	0.57	0.74	0.77	0.74

Table 6 Flood risk classifications

| Ponding depth (m)	0–30 min	More than 30 min
0.15–0.30 m	Low risk	Medium risk
0.30–0.50 m	Medium risk	High risk
More than 0.5 m	High risk	High risk
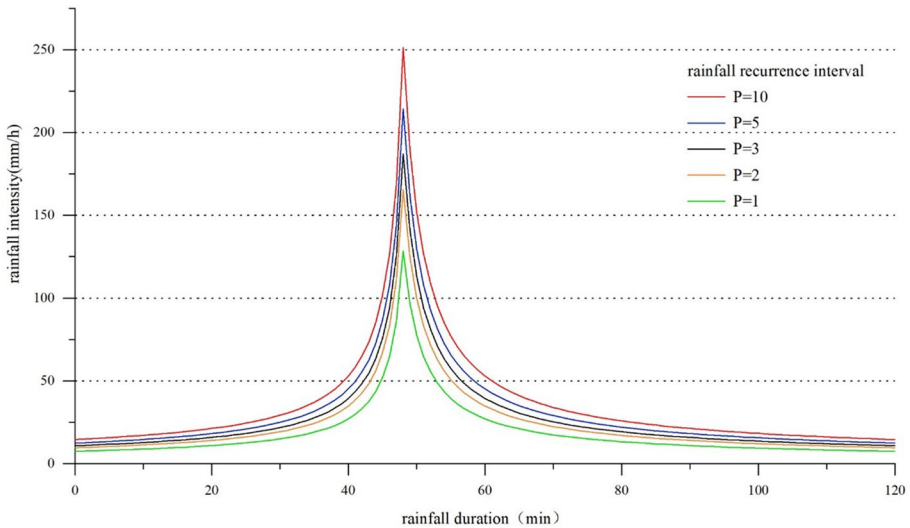
Fig. 6 Simulated rainfall patterns for the 1-, 2-, 3-, 5-, and 10-year return periods

Using the model simulation, rainstorms in the study area with recurrence periods of 1, 2, 3, 5, and 10 years were simulated, and a rainstorm pattern was generated using the rainstorm intensity formula (Fig. 6). The flood risk areas within the study area were identified for the different return periods to evaluate the flood risk in the area. As shown in Fig. 7, a higher rainfall return period is associated with greater rainfall and a greater flood risk.

As shown in Fig. 7, the flood risk was expressed visually on the map to determine the flood risk scenarios for certain locations. Because of factors such as delayed data updates, underground drainage pipe network data from 2015 are lacking; therefore, the current 2020 pipe network data were adopted for the simulation. As shown in Table 7, 15% of the study area showed a low risk, 53% of the study area showed a medium risk, and 32% of the study area showed a high risk. When the risk area proportion is large, flood disasters occur more easily. In addition, with continuous urbanization, flood risks in other areas increase annually.

4.2 Variations in flood risk with different underlying surface conditions

To generalize the underlying surface in the study area, it was divided into three main underlying surfaces: green space, building, and road. Then, 13 different underlying surface permeability rates were set by using the equal ratio example method to simulate the area percentage of permeability from 0 to 60% and to study the characteristics of flood risk
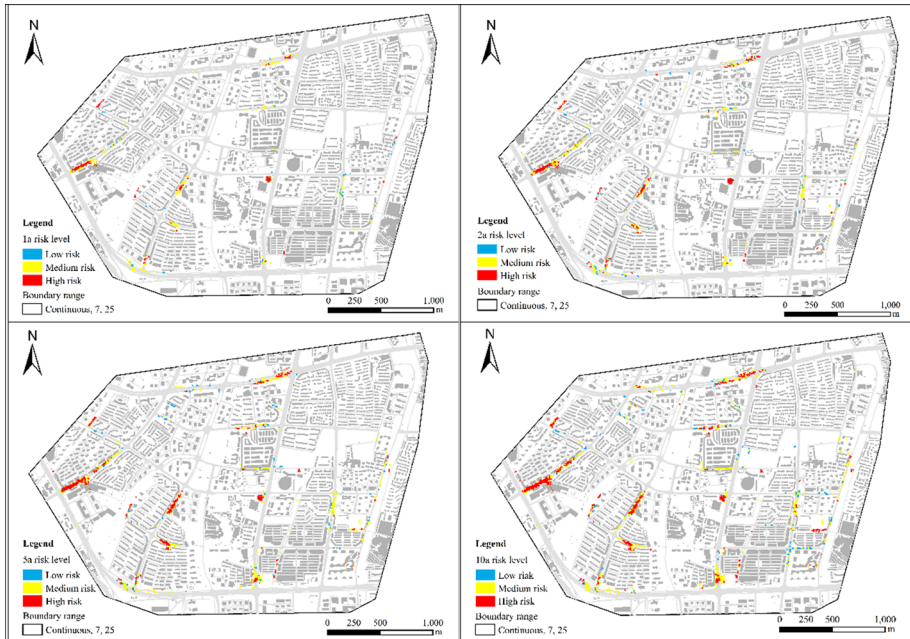
Fig. 7 Simulated flood risks for the 1-, 2-, 5-, and 10-year return period rainfall

Table 7 Risk areas and their proportions in the year of 2020 flood simulation

Risk level	Area (m²)	Percentage of risk area in total area (%)
Low risk	38,314.325	15
Medium risk	140,484.422	53
High risk	84,382.154	32

variations under different underlying surface permeability rates. The runoff generation and concentration models were set, respectively, according to the permeability of the underlying surface. For the buildings and roads, the fixed runoff coefficient method was adopted; the concentration parameter was 0.015; the initial loss type was the absolute value; for the runoff coefficient of the green space, the Horton coefficient was adopted; the initial permeability was 227 mm/h; the stable permeability was 110 mm/h; and the Horton attenuation coefficient K was 2. The simulation results were obtained by the operation model.

Figures 8 and 9 show the flood risk under the condition of 0–60% water permeability. A risk value of 0.01–0.30 indicates a low-risk area, meaning that the flood has a small impact on pedestrian travel; a risk value of 0.30–0.50 indicates a medium-risk area, meaning that the water in the road area may block vehicle traffic; values higher than 0.50 indicate a high-risk area. Areas with low terrain and insufficient drainage capacity can experience disasters such as house inundation, resulting in loss of personnel and property. It can be seen from the figure that as the permeability of the underlying surface increases from 0 to 60%, the area with ground ponding gradually decreased and the portion of high-risk areas became smaller. In addition, the areas with different flood risk levels were statistically
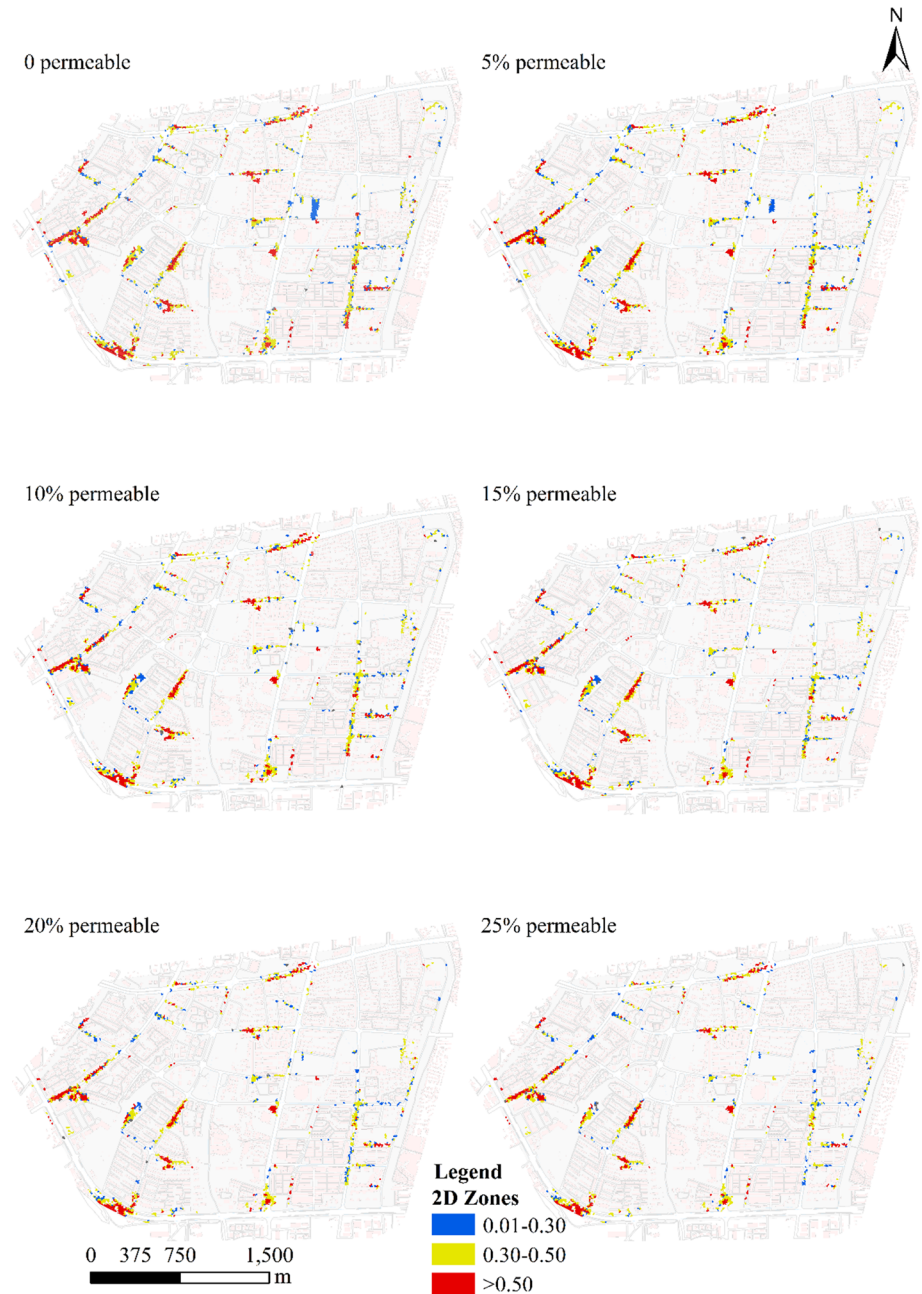
Fig. 8 Flood risks for 0–25% permeable surfaces

analyzed to compare the risk changes between 0 and 60% permeability. Referring to the flood depth–loss curve of Shanghai construction area, combined with the current construction status and topographic elevation distribution of Runcheng south area, the weight is

**Fig. 9** Flood risks for 30–60% permeable surfaces

Table 8 Permeabilities and risk areas of the different underlying surfaces

Proportion of permeable area of underlying surface	Low-risk area (m²)	Medium-risk area (m²)	High-risk area (m²)	Total risk area (m²)	Total risk score	Descent rate of total risk score
0	69,824.4	143,797.5	99,654.6	315,150.3	558,602.4	0.0
5%	62,382.6	137,868.2	91,899.1	294,426.8	524,194.1	6.2%
10%	54,710.6	126,599.6	85,617.1	270,029.0	482,245.7	13.7%
15%	49,858.6	116,782.1	78,660.3	247,507.1	442,949.5	20.7%
20%	48,047.3	104,848.2	73,191.9	229,114.9	407,155.0	27.1%
25%	41,879.9	94,288.5	66,993.4	205,424.0	366,705.9	34.4%
30%	40,333.2	80,853.6	61,202.3	184,559.2	326,615.2	41.5%
35%	29,587.5	75,559.4	57,209.5	163,708.6	296,477.5	46.9%
40%	30,351.5	64,783.2	50,683.0	146,909.6	262,375.8	53.0%
45%	25,855.5	56,811.8	43,668.7	127,300.1	227,780.7	59.2%
50%	21,999.4	51,183.0	36,600.5	111,113.9	198,897.4	64.4%
55%	19,404.0	44,883.0	29,926.5	95,234.3	170,043.8	69.6%
60%	13,718.4	39,900.5	24,006.2	79,286.8	143,193.5	74.4%

expressed by the loss coefficient of construction area. 0.01 was selected as the weight for low-risk areas, 0.03 as the weight for medium-risk areas, and 0.06 as the weight for high-risk areas. The total risk calculation formula (Eq. 10) was used to calculate total risk value as shown in Table 8.

As the permeability of the underlying surface increased from 0 to 60%, the risk of flood disaster decreases gradually, showing an evident law, the area with ground ponding gradually decreased and the portion of high-risk areas became smaller. The medium-risk area is much larger than the low-risk and high-risk areas, that is, the medium-risk area is the largest and the probability of medium risk is the largest; this indicates that the ability to resist medium-level flood disasters is extremely inadequate in this area.

From the proportion of areas under the three grades of flood risk, as shown in Fig. 10, it can be seen that the medium-risk area is significantly larger than high-risk area, followed by the low-risk area. When the permeability of the underlying surface is zero, the total flood risk area is 315,150.33 m^2 and the total risk value is 558,602.386. When the water permeability of the underlying surface is 35%, the total flood risk area is 163,708.601 m^2 and the total risk value is 296,477.505. When the water permeability of the underlying surface is 60%, the total flood risk area is only 79,286.79 m^2 and the total risk value is 143,193.462. Table 8 shows the permeability of underlying surface increases from 0 to 35%, and the reduction rate of flood risk is 46.9%; The water permeability increased from 35 to 60%, the flood risk disaster reduction rate was 27.4%, and the flood risk disaster reduction rate was almost halved. As shown in Fig. 11, the first curve represents the change trend of the total flood risk value obtained by simulation. The second straight line is the result of extending the change trend of the permeability from 0–35 to 60%. It can be seen that when the total flood risk value changes according to the attenuation trend of the permeability of 0–35%, its result is almost a straight line. Moreover, the attenuation coefficient of this straight line is greater than that of the part with water permeability of 35–60%, which indicates that the risk increase rate of the part with water permeability of 0–35% is greater than that of the part with water permeability of 35–60%. Therefore, it can be concluded that the flood risk rate will be higher when the permeability of the underlying surface is lower than 35%.
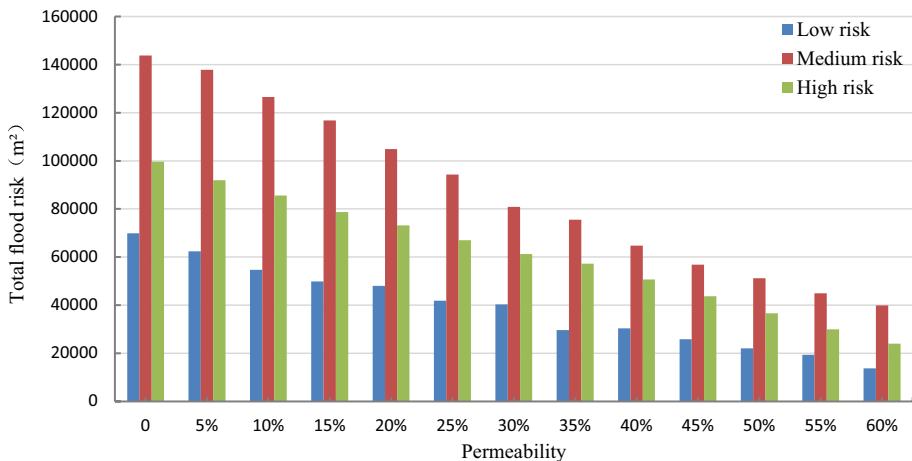
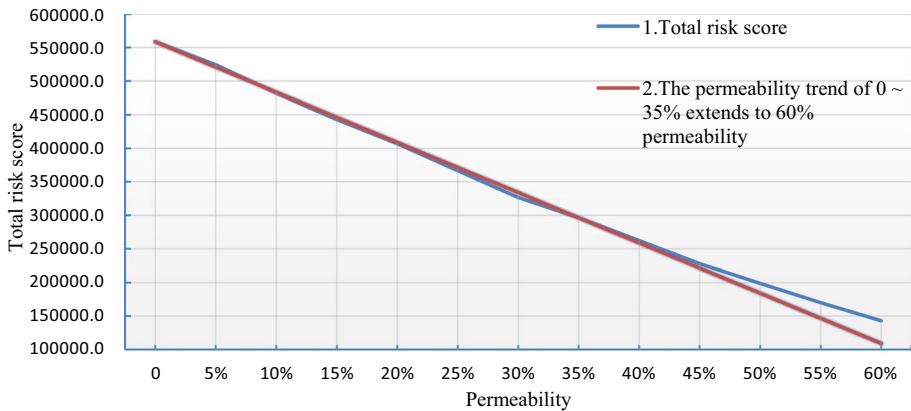**Fig. 10** Total flood risks at different surface permeabilities

Fig. 11 Variations in total flood risk for different surface permeabilities

5 Discussion

The increase in urban waterlogging risk is not only related to the permeability of the underlying surface, but also related to the terrain, composition, and distribution of the underlying surface. This paper only varied the permeability of the underlying surface to study the impact of the permeability on the risk of waterlogging. In the experiment, the permeabilities of 13 underlying surfaces (0–60%) were set through the equal difference method to simulate the changes in the underlying surface during the process of urbanization and evaluate its impact on urban flood risk. Predecessors have found that the increase in the impervious surface area reduces the total infiltration of water from the surface; the composition and distribution of underlying surface are related to urban waterlogging risk. Most studies on urban flood disasters are based on model simulation, and there are few cases to study flood disaster by controlling the permeability of underlying surface. Some studies have discussed the relationship between impervious surface and the spatial pattern of urban waterlogging risk points (Li et al. 2015). In this experiment, the infiltration rates in the green spaces and bare soils in the south area of Kunming were measured by the double-loop instrument experiment, which localizes the simulation parameters, resulting in simulation results more suitable to the local situation. Looking for data, few scholars localized the infiltration rate parameters of Kunming. In the infiltration rate experiment, it was also found that when measuring the infiltration rate for bare soil, the outer ring of the double-ring instrument could not damage the surface of bare soil, and the inner and outer rings need to maintain good tightness, and otherwise, the water of the inner ring leaked to the outer ring, causing the measured infiltration rate of the inner ring to be high.

During modeling and simulations, although the data processing method of the basic pipe network was simple, time and energy were required. Whether the data processing of the basic pipe network was appropriate is related to water accumulation after operation of the entire model. The watershed method also had major influences on model operation, including the manual partitioning of a subset of the watershed and use of a Voronoi diagram, which led to large differences. The manual subset of watersheds has many limitations that may lead to no water and watershed model convergence problems, whereas such issues rarely occurred when using the Voronoi-derived divisions. The accuracy of the simulation was also largely related to the parameters used in the

model. A major contribution of this experimental study was obtaining localized parameters using field measurements and then applying them to the model to produce more accurate results.

6 Conclusions

In this study, we construct a one-dimensional and two-dimensional coupled drainage flood model through InfoWorks ICM, control the water permeability of urban underlying surface, simulate the urban flood risk change of Runcheng south area of Kunming under the continuous change of underlying surface between 2012 and 2020. The relationship between urban flood and underlying surface in the process of urbanization is analyzed. The permeability of the underlying surface is an important factor affecting urban flood. The risk increase rate of the part with permeability of 0–35% is greater than that of the part with permeability of 35–60%. When the permeability of the underlying surface is lower than 35%, the flood risk rate will be higher. Therefore, the water permeability of the urban optimal underlying surface shall not be less than 35% and shall be maintained at more than 30%, because once the urban water permeability is less than 35%, the risk rate of flood disaster will increase rapidly, which will aggravate the urban flood disaster.

The influences of different rain types on flooding with the same underlying surface permeability, as well as the influence of different underlying surfaces with the same rainfall type on flooding, were analyzed. In addition, the influence of the underlying surface on flooding with the evolution of urban construction was assessed. Although it is accepted that urban underlying surfaces can aggravate flooding, the specific impacts are not completely clear. Furthermore, we determined that based on the simulation of historical rainfall conditions, urban flood disasters over many years can be compared, the formation of water accumulation locations can be determined, and relationship between the changes in green land rate and floor area ratio and changes in water accumulation can be analyzed. Such analyses can reflect the influence of the underlying surface on flooding caused by the evolution of urban construction. By simulating underlying surface ratio conditions, the water accumulation degree of different underlying surfaces in daily rainfall conditions can be compared. Combined with the localization parameters from Kunming City and combined analytical results of various conditions, simulations can provide suggestions and help control plot ratios and green land rates in urban development.

Declaration

Conflict of interest The authors declare that there is no conflict of interest.

References

Abulkadir A, Wuddivira MN, Abdu N et al (2011) Use of Horton infiltration model in estimating infiltra-tion characteristics of an Alfisol in the Northern Guinea Savanna of Nigeria. J Agric Sci Technol 6:925–931

Bisht DS, Chatterjee C, Kalakoti S, Upadhyay P, Sahoo M, Panda A (2016) Modeling urban floods and drainage using SWMM and MIKE URBAN: a case study. Nat Hazards 84(2):749–776. https://doi.org/10.1007/s11069-016-2455-1

Chakraborty S, Mukhopadhyay S (2019) Assessing flood risk using analytical hierarchy process (AHP) and geographical information system (GIS): application in Coochbehar district of West Bengal, India. Nat Hazards 99(1):247–274. https://doi.org/10.1007/s11069-019-03737-7

Chen T, Xia MM, Liu YP, Che AW (2020) Regulation of stormwater runoff in sponge reconstructed community based on SWMM. China Water Wastewater 36(11):103–111

Cheng T, Xu Z, Hong S, Song S (2017) Flood risk zoning by using 2D hydrodynamic modeling: a case study in Jinan City. Math Probl Eng 2017:5659197. https://doi.org/10.1155/2017/5659197

Feng B, Zhang Y, Bourke R (2021) Urbanization impacts on flood risks based on urban growth data and coupled flood models. Nat Hazards 106(1):613–627. https://doi.org/10.1007/s11069-020-04480-0

Geng Y, Zheng X, Wang Z, Wang Z (2019) Flood risk assessment in Quzhou City (China) using a coupled hydrodynamic model and fuzzy comprehensive evaluation (FCE). Nat Hazards 100(1):133–149. https://doi.org/10.1007/s11069-019-03803-0

Hossain Anni A, Cohen S, Praskievicz S (2020) Sensitivity of urban flood simulations to stormwater infrastructure and soil infiltration. J Hydrol 588:125028. https://doi.org/10.1016/j.jhydrol.2020.125028

Hou ZM (2019) Research on engineering case of double-loop seepage test in groundwater environmental impact assessment of a chemical project in Tianjin. Ground Water 44(04):26–28

Hou JW, Du YX (2020) Spatial simulation of rainstorm waterlogging based on a water accumulation diffusion algorithm. Geomat Nat Hazards Risk 11(1):71–87

Hu S, Cheng X, Zhou D, Zhang H (2017) GIS-based flood risk assessment in suburban areas: a case study of the Fangshan District, Beijing. Nat Hazards 87(3):1525–1543. https://doi.org/10.1007/s11069-017-2828-0

Huang M, Jin S (2019) A methodology for simple 2-D inundation analysis in urban area using SWMM and GIS. Nat Hazards 97(1):15–43. https://doi.org/10.1007/s11069-019-03623-2

Huang GR, Wang X, Huang W (2017) Simulation of rainstorm water logging in urban area based on InfoWorks ICM model. Water Resour Power 35(02):66–70, 60

Keifer CJ, Henry HC (1957) Synthetic storm pattern for drainage design. J Hydraul Res 83(4):1–25

Kong F, Sun S, Lei T (2021) Understanding China's urban rainstorm waterlogging and its potential governance. Water 13(7):891

Li BY, Zhao YL, Fu YC (2015) Spatio-temporal characteristics of urban storm waterlogging in Guangzhou and the impact of urban growth. J Geo-Inf Sci 17(04):445–450

Li Y, Di SC, Zhu YH, Li YK, Zhang YH, Xu JM (2019) Multi-view analysis of urban flood based on multimodel coupling. China Rural Water Hydropower 5:82–90

Li JZ, Li CQ, Wang FS, Zhang YW (2020) An urban storm flood model based on cellular automata. China Rural Water Hydropower 11:73–76, 82

Liang JH (2016) Brief analysis of application program of optimization design of waterlogging monitoring system for the Pearl River Delta cities. Pearl River 37(6):66–69

Liu J, Shao W, Xiang C, Mei C, Li Z (2020) Uncertainties of urban flood modeling: influence of parameters for different underlying surfaces. Environ Res 182:108929. https://doi.org/10.1016/j.envres.2019.108929

Meng X, Zhang M, Wen J, Du S, Xu H, Wang L, Yang Y (2019) A simple GIS-based model for urban rainstorm inundation simulation. Sustainability 11(10):2830

Peng J, Liu Y, Shen H, Xie P, Hu XX, Wang YL (2016) Using impervious surfaces to detect urban expansion in Beijing of China in 2000s. Chin Geogr Sci 26:229–243

Qi W, Ma C, Xu H, Chen Z, Zhao K, Han H (2021) A review on applications of urban flood models in flood mitigation strategies. Nat Hazards 245:1–32. https://doi.org/10.1007/s11069-021-04715-8

Quan R-S (2014) Rainstorm waterlogging risk assessment in central urban area of Shanghai based on multiple scenario simulation. Nat Hazards 73(3):1569–1585. https://doi.org/10.1007/s11069-014-1156-x

Rong Y, Zhang T, Zheng Y, Hu C, Peng L, Feng P (2020) Three-dimensional urban flood inundation simulation based on digital aerial photogrammetry. J Hydrol 584:124308

Seenu PZ, Venkata Rathnam E, Jayakumar KV (2019) Visualisation of urban flood inundation using SWMM and 4D GIS. Spat Inf Res 28(4):459–467

Shi Y (2012) Risk analysis of rainstorm waterlogging on residences in Shanghai based on scenario simulation. Nat Hazards 62(2):677–689. https://doi.org/10.1007/s11069-012-0099-3

Sun B, Xie SB, Wang ZY, Wu HY, Liu H (2020) Shenzhen City waterlogging prevention based on multiple LID schemes. Yangtze River 51(6):17–22

Wang SJ (2018) Evaluation of drainage capacity of urban drainage network based on infoworks ICM. J Green Sci Technol 18:156–159

Wang JJ, Wang CT, Zeng S (2020a) Assessment of urban drainage capacity and waterlogging risk based on scenario simulation. China Water Wastewater 36(17):115–120

Wang XY, Zhou Y, Yu JN (2020b) Evolution of green infrastructure layout and waterlogging risk assessment based on cellular automata simulation of urban expansion: a case study of Wuhan City. Landsc Archit 27(11):50–56

Xia J, Zhang Y, Ling CM, Liu J (2018) Review on urban storm water models. Eng J Wuhan Univ 51(2):95–105

Xu B, Lei XH, Wang H, Kang AQ (2019) Research on urban flooding simulation in a coastal city based on SWMM model. J China Inst Water Resour Hydropower Res 17(3):211–218

Yin J, Ye M, Yin Z, Xu S (2015) A review of advances in urban flood risk analysis over China. Stoch Environ Res Risk Assess 29:1063–1070

Yu H, Zhao Y, Fu Y, Li L (2018) Spatiotemporal variance assessment of urban rainstorm waterlogging affected by impervious surface expansion: a case study of Guangzhou, China. Sustainability 10(10):3761

Zhu X, Zhou B, Qiu X, Zeng Y, Ren W, Li S, Wang Y, Wang X, Jin Y (2019) A dynamic impact assessment method for rainstorm waterlogging using land-use data. J Integr Environ Sci 16(1):163–190

Publisher's Note Springer Nature remains neutral with regard to jurisdictional claims in published maps and institutional affiliations.